Developed emulsification in porous media flow

Ahmad Kharrat[1], Bianca Brandstätter[1], Mostafa Borji[1], Gerhard Fritz-Popovski[2], Oskar Paris[2], and Holger Ott[1,]*

1 Department Petroleum Engineering, Montanuniversität Leoben, 8700 Leoben, Austria.
2 Institut für Physik, Montanuniversität Leoben, 8700 Leoben, Austria.

Abstract. With the use of surfactants, the interfacial tension between oil and water can be lowered to a degree that solubilisation of oil by the injection water leads to a near-miscible displacement. The resulting type of emulsion, however, depends on the way how the two phases contact each other and ultimately on the mixing, respectively flow regime. While mixing can be turbulent in classic test tube experiments, under laminar flow conditions in porous media the miscibility can develop slowly over time, depending on the dispersion mechanisms that facilitate the contact between the phases. The present study investigates this developed miscibility during surfactant flooding. We perform microfluidic experiments with generic oil and surfactant solutions in a wide salt concentration range across optimum displacement conditions. The study shows that in addition to a classic immiscible displacement, oil is increasingly solubilized and transported in a phase with a foam-like texture that develops from a drop-traffic flow. The extend and the stability of those phases depends on the salinity and hence of the efficiency of the surfactant solution.

1 Introduction

Oil and water are usually immiscible. Almost miscible conditions can, however, be facilitated by the addition of surface-active components - surfactants - which can settle on the oil-water interfaces and reduce the interfacial tension between the two liquids [1]. In this way, stable emulsion phases can form. In different scientific areas emulsions, their formation and stability play a decisive role and are investigated [2] [3] [4] [5]. Although our understanding of emulsion formation has improved, important connections are still missing, especially the connection of emulsification under various mixing or flow conditions.

In recent years, pore scale studies on mixing behavior and emulsification appeared [6] [7] [8] [9]. The in-situ formation of microemulsions from generic fluid systems was investigated in T-junctions by variation of the salt content of the aqueous phase [10]. The work was continued by examining emulsification in dead-end pores. It has been found that phase behavior alone is insufficient to predict emulsification under dynamic conditions, and that the flow rate controls emulsification [11]. The influence of the exact pore space geometry was investigated using three different microfluidic pore patterns [12]. The work was repeated, but using a radial flow geometry while focusing on the displacement stability based on the microemulsion type and particle size, which significantly impact the displacement efficiency [13]. The results show that the observed flow regimes follow the equilibrium phase behavior, i.e. that dimensionless scaling parameters based on equilibrium emulsion properties explain the observed displacement patterns.

Generally, emulsion phases can be classified by their particle sizes into macro (loose) and micro (tight) emulsions, which differ by the latter being thermodynamically stable.

Another classification scheme was introduced by Winsor defining three emulsion types: Type I – oil-in-water emulsion, Type II – water-in-oil emulsion, and a Type III [14]. Type III forms a third phase at the interfave between oil and water, characterized as microemulsion. Type III is considered as the optimum condition in displacement physics. Especially the optimum has been intensively investigated in the oil and gas industry with regards to enhanced oil recovery (EOR) [15] [16] [17].

However, the situations may be different if surfactants are generated in-situ, like in alkaline flooding. Due to the wide variety of acidic crude-oil components, in-situ saponification of crude by alkaline solutions may lead to surfactants with a wide variety of molecular properties, predominantly characterized by the wide size and property distribution of their lipophilic tails. In such situations, the variation of brine salinity may not lead to clear optimum conditions since molecular properties are too different to match with a global tuning parameter. However, displacements outside the optimum can lead to the formation of complex fluid textures on a pore scale leading to complex displacements [9].

In order to understand displacements outside the optimum, we study a generic oil-water-surfactant system in the over- and under-optimum by tuning injection water salinity in a wide concentration range across the optimum condition. Sub-optimal conditions can also be of interest for surfactant flooding, since salinity variations due to dispersive effects in porous-media flow, likely lead to salinity variations – the system may be locally outside the optimum. In this context, we investigate the spatial and temporal development of emulsion phases in microfluidics by means of optical and quantitative-fluorescence microscopy. We observe the actual mechanisms of oil mobilization and displacement with a particular interest in the question of the comparability of emulsification in classic ex-situ experiments and under flow conditions in porous media.

---

* Corresponding author: holger.ott@unileoben.ac.at

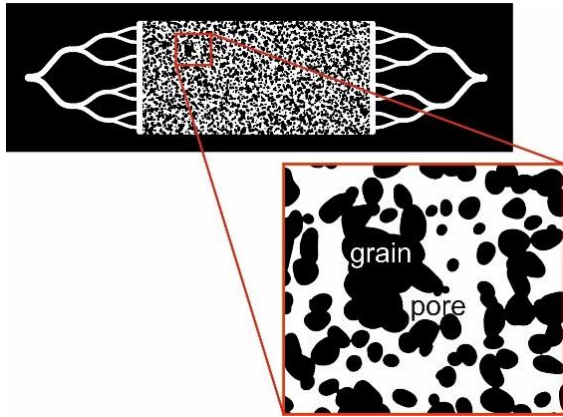## 2 Materials and Methods

2.1. Microfluidic chip – the porous medium

Figure 1 : 2D pore structure etched in glass microfluidic chips. The porous domain is 2×1 cm^2 in size and is contacted on the left and right by channel systems for fluid injection and production resulting in a linear flow geometry.

Experiments were performed with microfluidic chips made from borosilicate glass, representing a 2D porous media. The pattern is characterized by a homogeneous etching depth of 20 μm and a lateral definition of pores and pore throats. Porosity and permeability have been determined to $\phi = 0.57$ and $K = 2.5$ D and total pore volume to 2.3 μl. The total porous domain is 2 cm × 1 cm with channel systems at the inlet and outlet for a proper fluid distribution and fluid collection as displayed in Figure 1. The lateral porous structure is rather open and homogeneous with all features larger than the etching depth. This microfluidic pattern has been used in earlier studies [9].

2.2 Fluids

Experiments were performed using decane (Sigma Aldrich, 99% purity) as oil phase. The injection water was based on deionized (DI) water with J13131 as surfactant, 2-Butanol as a cosolvent, and sodium chloride in different concentration as tuning parameter. This surfactant cocktail was used in earlier studies as well [12] [13]. The chemicals are given in Table 1. Since both fluids, water and decane are transparent and optically indistinguishable, contrast agents were added to achieve optical and fluorescence contrast between them. For the optical contrast, the colorant Sudan II was added to the oil phase, which resulted in a brownish color. As fluorescence agent, a fluorescence sodium salt was added to the aqueous phases. The influence of the contrast agents on the IFT and phase behaviour was studied; no significant influence was observed for the given concentrations.

Table 1 : Chemicals used in this study.

Chemical	Concentration	Source
J13131	0.5 wt.%	Shell
2-Butanol	2 wt.%	Sigma Aldrich
NaCl	1 to 5 wt.%	Sigma Aldrich
Fluorescent salt	100 mg/l	Sigma Aldrich
Sudan II	10 mg/l	Sigma Aldrich

The combination of the optical and fluorescence microscopy allowed to separate the phases. In the combined data set, it turned out that the Sudan II does not detectably participate in the emulsion phase, which helped to identify specific features in the observed macro structures. At the same time, the fluorescence salt scales nicely with the amount of oil in aqueous phase, even to very high oil content, but did not participate in the pure oil phase. Therefore, both agents deliver complementary information on the fluid-fluid system.

2.3 Instrumentation

Leica DMi8 microscope with fluorescence filter was used to capture high quality and detailed optical and fluorescence images of porous domain and the fluids therein. The images were acquired from the entire domain by an integrated wide-range automated XY table in combination with a stitching software. The images were recorded with a Leica DMC2900 camera and a pixel size of 1.8 μm. The temporal resolution of the individual image was given by the acquisition time of 1 ms in optical, and 2 ms for fluorescence microscopy. The overall time resolution was limited by the XY scanning to about 30 s, and 150 s, respectively. In some cases, videos were taken for smaller regions of specific interests.

Fluids were injected with a high precision Chemyx Fusion 200 syringe pump. For each fluid type, a separate syringe was used. On the downstream side, a constant pressure boundary condition was realized by producing fluids into a vessel at atmospheric pressure. For preparation purpose, a vacuum pump was installed on the downstream side to evacuate the micromodel and the flow lines, and for pre-saturation.

2.4 Experimental Procedure

The initial state of all experiments was a fully oil saturated porous domain, i.e., $S_{o,i} = 1$. The flooding experiments were performed at stabilized ambient temperature and ambient pressure with a constant flow rate boundary condition at the inlet, and a constant pressure boundary condition at the outlet. In all shown images, the flooding direction is from left to right. Surfactant solutions were injected for about 60 hours, with an injection rate of 0.002 ml/h (corresponding to a Darcy velocity of (~1 ft/day)), resulting in ~50 pore volumes (PV) injected in total. The experiments were stopped at times where no changes in the remaining oil saturation could be detected.

The images were captured in tiles with a small field of view, covering altogether the total domain after stitching.

The small field of view allows for high spatial resolution to observe emulsification and displacement processes on a sub-pore scale.

After each experiment, the chip was flushed with a sequence of 3 ml water and decane to dissolve the remaining salt, surfactant and dying agents in the system. Afterward, 2 ml of acetone was injected to miscible displace the remaining fluids (mainly water), and in the last stage, a vacuum was applied for at least 4 hours to remove the acetone from the system. All the steps were observed by microscope to ensure the quality of the cleaning procedure.

3 Fluid-Fluid Interactions

The fluid-phase behavior was characterized using various standard methods. The tuning parameter for optimizing phase behavior is typically the salinity, in the present case the NaCl concentration, which we vary between 1 and 5 wt.%.
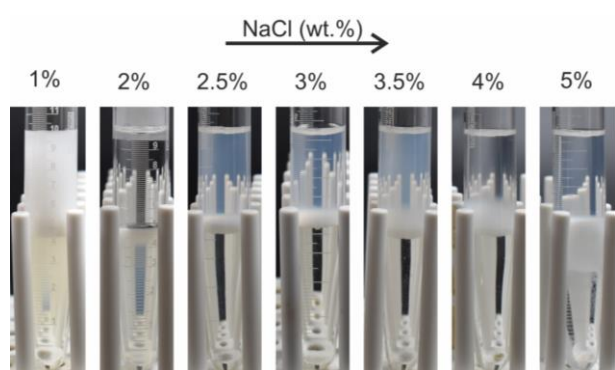
3.1 Test-tube experiments

Figure 2: test-tube phase behavior experiments of a decane-surfactant solution system with increasing NaCl concentration.

Oil and surfactant solutions were contacted in glass test tubes with equal volumes of 5 ml of both fluids. To guarantee the quality of the volumes and to minimize the interactions between the fluids prior to the mixing step, we first filled the test tubes with 5 ml of the aqueous from bottom to top and then added 5 ml of oil by using a high-precision syringe pump. The fluids were then mixed by a tube rotator (Fisherbrand^{TM}, USA) for 24 hours at 25 rpm. Afterward, the tubes were placed vertically at stabilized ambient temperature to reach its equilibrium gravity-separated phases. Images were taken during and in the final stage of the separation process. The images of the final equilibrium state are shown in Figure 2. The tests were reproduced in repeat experiments.

Since we are interested in displacements outside optimum conditions, the steps in which the NaCl concentration increased are rough and the concentration range is wide. Optimum conditions can be assumed to be in between 2 wt.% and 2.5 wt.% where the upper and lower phase are relatively clear, and the behavior changes from a lower slightly blurred phase to a blurring of the upper phase. The principal behavior has been reproduced with the optical and fluorescence contrast agents in the respective phases.

3.2 Nano structures of emulsion phases

In the phase behavior experiments, milky and transparent phases were observed. A transparent phase may indicate a pure fluids phase. However, microemulsions may be transparent as well, if the particle sizes are smaller than the wave length of light. To further understand the observed phases, some of the phase-behavior experiments were repeated in small-scale tubes (Mark tubes) suitable for small-angle X-ray scattering (SAXS). With SAXS, fluid particle, respectively bubbles of nm size are accessible.

As for the classical phase-behavior experiments discussed above, equal volumes of both phases were dosed in test tubes, the tubes were sealed and mixed by shaking. The mixture was then filled in the mark tubes and sealed. In such small-size tubes, gravity separation is supressed. As for the classical tests, clear and milky phases are visually observed. In case of 2 wt.% NaCl, a single homogeneous phase is observed as may be expected near the optimum without gravity separation. At all other concentrations, milky and clear phases were observed.
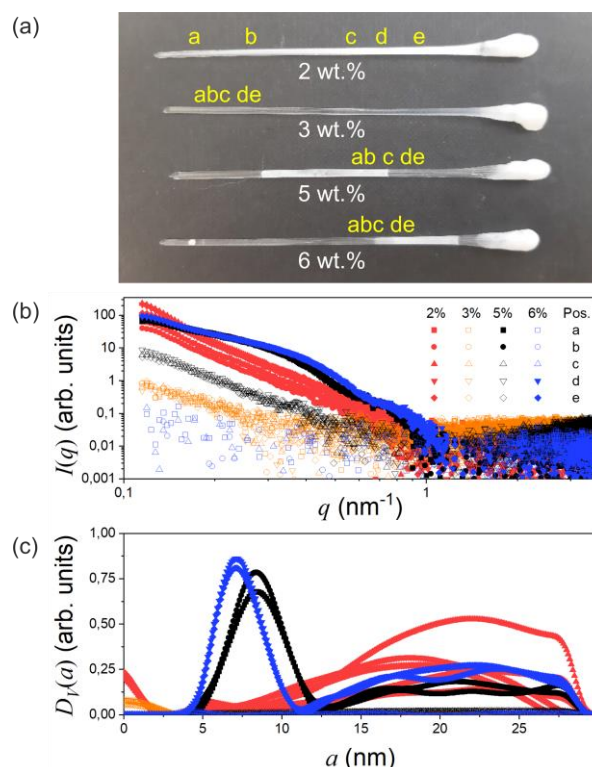

Figure 3 : SAXS measurements to determine micro structures in emulsions. (a) Small-scale test tubes with indicated NaCl concentration and positions at which SAXS measurements were taken. (b) SAXS curves for the concentrations and positions indicated in (a). (c) Size distributions calculated from the scattering curves in (b).

SAXS measurements were performed using a Bruker Horizon-N8 (Bruker-AXS, Germany) equipped with a IμS micro-focus source (INCOATEC, Germany) and a VÅNTEC 500 detector (Bruker-AXS, Germany). Copper Kα radiation was used. The samples were moved in an oscillating way along the capillary's axis in order to average a larger sample volume.

Figure 3 shows details of the experiment. The test tubes with the samples and the positions at which measurements were taken are marked in image (a). Scattering curves are shown in panel (b) as function of the wave vector q. Untextured fluids are expected to show a pure q^{-4} behavior while fluid with texture in the sensitivity range up to ~30 nm show features like shoulders and deviating slopes in the double logarithmic plot. From these features, a particle size distribution can be calculated. Additionally, pure decane and aqueous solutions have been measured in order to correct for the background in the scattering signal. By background correction, the scattering signal from the emulsion phases can be isolated.

The observations may be split in scattering responses from clear and milky phases; in the accessible particle size range, only the milky phases responded, and the clear phases appear as untextured.

The scattering curves have been transformed into size distributions assuming globular particles (Figure 3 (c)). The distributions show that all observed milky phase contain particles in a wide range of radii above 10 to 15 nm. The size distribution is artificially truncated (sharp drop at ~28 nm) by the accessible size range of the measurement, and is likely to continue. The samples with higher NaCl concentrations – 5 and 6 wt.% – show a distinct additional contribution with smaller particle radii peaking in between 7 and 12 nm with a rather narrow distribution.

The measurements show, that observed milky phases may be considered as microemulsions. However, larger scale textures in and above the size of the wave length of light can be assumed, otherwise the phases should appear optically transparent. These sizes are out of sensitivity range of the SAXS measurements. The clear phases, on the other hand, appear as untextured.

4 Displacement Mechanisms at sub- and near-optimal conditions

4.1 Flooding experiments

Displacement experiments were performed in microfluidics to study the displacement efficiency and also the effect of in-situ emulsification. In this study, we focus on the simplest process, which is water injection in an initially oil saturated domain, i.e. surfactant flooding in a secondary recovery mode. Such flooding experiments have been performed for NaCl concentration in between 1 to 5 wt.%, with otherwise leaving the overall composition of the aqueous phase constant. Figure 4 shows a typical flooding sequence for 4wt.% NaCl, i.e., in the over optimum. In the left column of Figure 4, the total flooding domain at different time steps from the water invasion in (a) to the time of breakthrough in (e) is shown. The light-blue phase is the pore space occupied by the invading aqueous solution, while the oil is colored in brown and the solid grains in white.
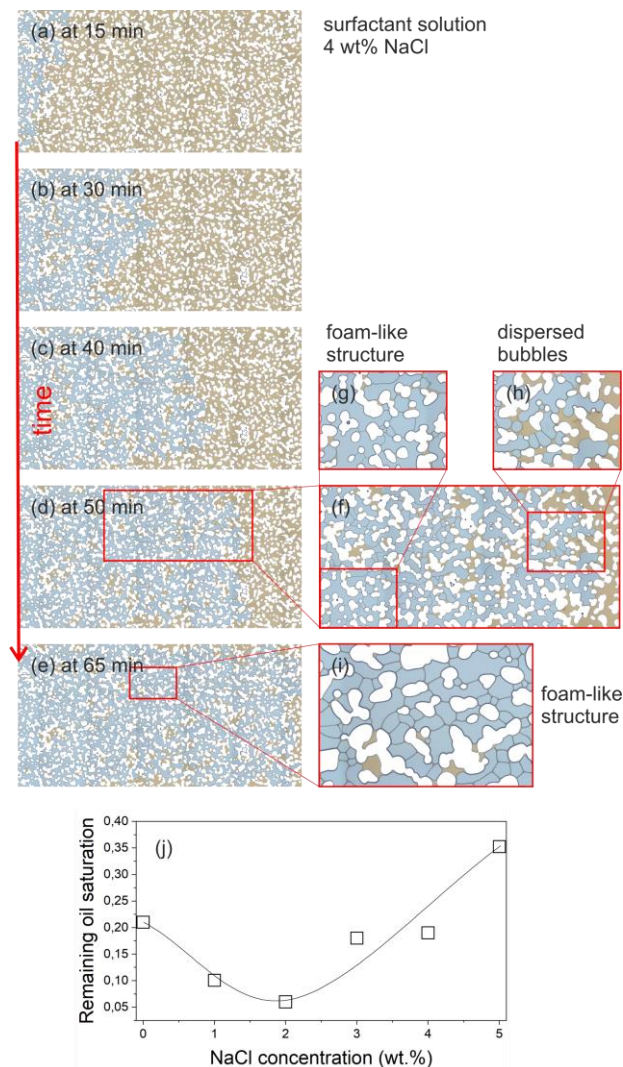

Figure 4 : (a) to (e) time series of an oil displacement process by a surfactant solution with 4 wt.% NaCl – in the over optimum. The phases are colored with white being the grains, blue the injection water, and brown the oil phase. (f) to (h) zoom images into the displacement front show the development from a loose emulsion of dispersed bubbles at the front into a foam-like phase further behind the front. (j) Remaining oil saturation as function of NaCl concentration. The data are taken right after breakthrough for comparability reasons.

Before going into details of displacements and emulsification, it is intuitive to discuss the displacement efficiency. Figure 4 (j) shows the remaining oil saturation right after breakthrough for experiments at different NaCl concentrations. The curve was calculated from the optically taken images considering only the desaturation of the pure oil phase marked by Sudan II as contrast agent (brownish phase in Figure 4). The optical contrast does not allow to detect the oil participating in the aqueous phase, since Sudane II does not participate in the emulsion with a detectable concentration. Defining the remaining oil saturation, respectively the recovery like this, the optimum concentration can be found at 2 wt.% NaCl.

What causes this difference in displacement efficiency and how is this related to emulsification processes in the pore space? The invasion process is similar to a primary drainage process, with the injection water being the non-wetting phase during the invasion. This be seen from the

contact angles right at the displacement front in Figure 4 (f) and (h). The wetting state is per definition a result of the initial saturation state ($S_{o,i} = 1$) with the solid surfaces being covered with oil, which forces the invading water into a classic drainage process. As illustrated in the same images, the injection water breaks in dispersed droplets and ganglia right at the displacement front leading to drop-traffic and ganglia flow. Right behind the displacement front, the aqueous phase appears disintegrated in droplets as well. There, the drops are very tightly packed and touch each other. However, there are clear boundaries between the droplets and there is no coalescence between them. From an emulsion point of view, dispersed water bubbles may be described as water-in-oil type with a dominant water content. In the dense packed phase, the boundaries between the droplets show similarity to a foam phase, with the boundaries being interpreted as lamella and vertices.
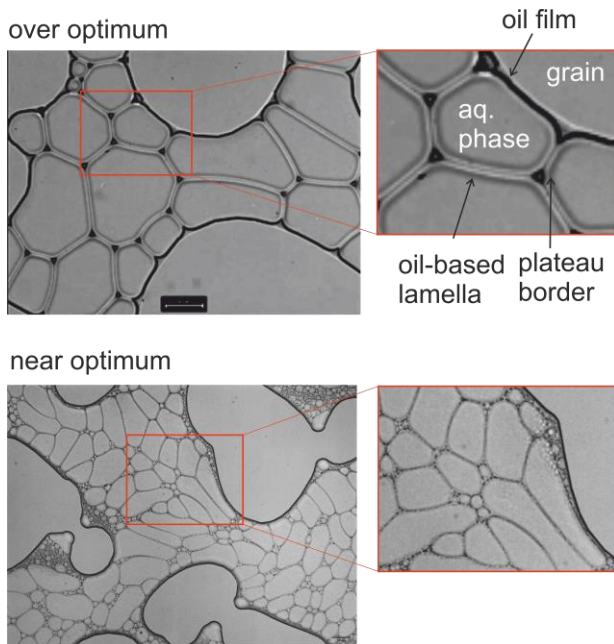

Figure 5 : Details of the foam-like phase in the over optimum (a) and at near-optimum conditions (b) salinity. The phases show all signatures of a foam texture.

In all experiments, sequences of dispersed bubbles/ganglia followed by a foam-like phase and followed by a rather connected, homogeneous aqueous phase can be observed from the front in downstream direction.

But why do we call this emulsion phase "foam like"? Typically, water-oil mixtures are not called foam. However, having a closer look to the emulsion texture, the similarity becomes striking. Figure 5 (a) shows zoom images on the sub-pore scale in the foaming regime at over optimum conditions. This phase shows all signatures of a foam and is as well flowing like a foam phase as illustrated in (supp. mat.) and further below in Figure 8; these textures may be compared to work on foam flooding in microfluidics [18] [19] [20]. In a quasi 2D porous media, planar 2D foam structures were found; water is the internal phase enclosed in oil-based lamella forming

closed compartments. The structure is triggered by the oil wet conditions of the solids, enabling the lamella to attach to the solid grains covered by oil films. The stabilizing function of the oil films becomes visible in the respective video sequence (supp. mat.). As in classical foam phases, vertices are formed connecting three lamellae with the (close to) 120-degree angles (for 2D structures).

At 2 wt.% NaCl, near the optimum, the texture changes and more complex structures can be observed. Due to the reduced IFT, the system is able to generate more interfacial area, resulting in a structure as shown in Figure 5 (b). The bubble-size distribution becomes broader with smaller bubbles at interfaces to the solid and in between the compartments.

4.2 Solubilization in fluorescence microscopy

Fluorescence microscopy provides additional information on the optically observed phase. What has optically been identified as aqueous phase in different droplets, ganglia or compartments, turned out to contain solubilized oil and is therefore an emulsion phase itself, but without optical contrast to the pure aqueous phase; the oil-in-place becomes solubilized by the surfactant solutions.
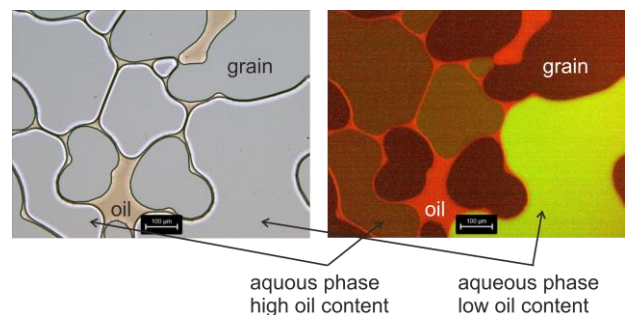

Figure 6 : Comparison of the information from optical microscopy (left image) and fluorescence microscopy (right image). The right image was recorded with a long exposure time.

Figure 6 illustrates that each aqueous compartment shows a different response to the fluorescence light, indicating micro emulsions, an optically homogeneous appearing phase, with different compositions, respectively oil content in water.

Figure 7 (a) shows the spatial variation of fluorescence intensity after breakthrough in the near-optimum case with 2 wt.% NaCl in the aqueous phase. The zoom image shows a reverse order of structures with the foam like phase in front of dispersed bubble phase. This is a result of step-wise mobilized remaining oil as will be discussed in the next section. From the textural point of view, the phases become more obvious. Because of the limited participation of the different used contrast agents, the lamella of the foam-like structure can be identified as oil phase, while the interior of the droplets and compartments seem to be aqueous-based, but with different solubilized oil content, depending on their history in moving through the oil saturated porous medium. The intensity of the fluorescent light is a measure of the water content in the

phase, and with this, the phase composition can be identified.
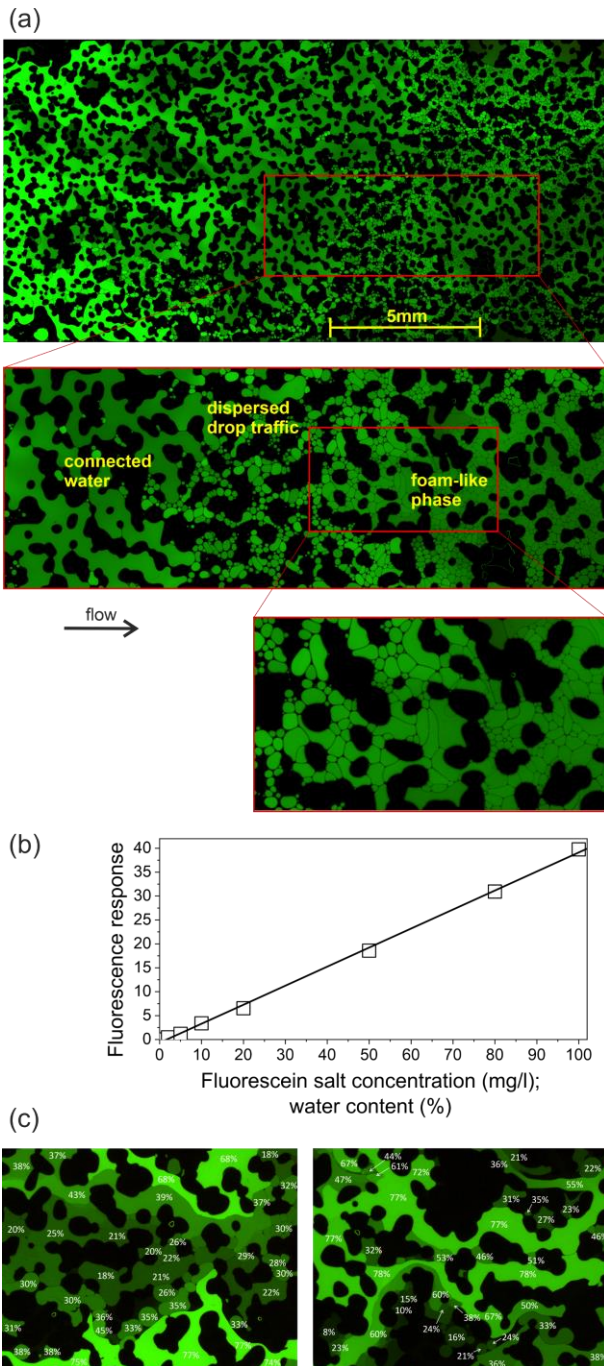

(a)

(b)

(c)

Figure 7 : (a) fluorescence-microscopy images at near-optimum conditions (2 wt.% NaCl). Due to the high contrast, the texture and the sequence is well represented in the images. (b) independently determined calibration curve linking the fluorescence response to the water content. (c) Images from a flooding experiments with 4 wt.% NaCl with a calibrated color scale. The numbers refer to the oil-in-water content: 100% would denotes a pure aqueous phase and 0% refer to a pure oil phase.

Figure 7 (b) shows a calibration curve with the fluorescence response as function of the Fluorescein-salt concentration. With the calibration, the oil content can be quantified. The images in (c) and are taken from a 4 wt.%-NaCl experiment and are labelled with the percentage of

water being in the phases. The exact spatial distribution is the first thing that is catching the eye. The individual compartments, representing foam cells or droplets, show a homogeneous intensity with a well-defined fluorescein concentration; each compartment seems to be isolated from the surrounding others maintaining partly the high compositional differences with a well-defined oil content in each compartment. The detected water fractions range from below 20% (above 80% oil) to the pure aqueous phase. This reflects a wide variation of emulsions, that may be labelled as microemulsions, since no structures are optically resolved within the compartments.

4.3 Interpretation

The observed foam-like structures suggest an interpretation of the observed macro (loose) emulsion phases in terms of foam formation. While foam is typically referred to gas-surfactant solution systems, we observe these structures in surfactant flooding, respectively in oil displacement processes. The structures outside the optimum develop continuously from a ganglion, respectively droplet flow to the foam-like flow. Due to this continuous transition and considering a foaming mechanism, we are able to explain the peculiarities in the drop-traffic flow and macro emulsion structures observed in earlier investigations [9]. Especially the fact that coalescence between adjacent – touching – water droplets is rare, may be related to the nature of the interfaces between those droplets. Our hypothesis is that those droplets already form a low-quality foam. Through time and distance, oil becomes solubilized (and displaced) and foam quality is increasing. The oil phase is then confined in the observed lamella, stabilized by surfactants and the classical competition of electrostatic repulsion at the interfaces and capillary forces in the vertices. The zoom image of Figure 7 (a) illustrates the similarity and the transition between the two types of structures, referring to foam quality as in the classical foam phase.

Those structures can be found for all NaCl concentrations, but are especially stable at over- and under-optimum conditions, where we can assume that the surfactant molecules are not efficiently used. This is exactly in analogy to the classical foam formation, where surfactants are needed for lamella stabilization, but as well for the adjustment of capillary suction. Under ultra-low IFT conditions, foam would collapse, because capillarity forces cannot prevent the swelling of the interface layers, respectively the lamella in foam phases. The further away for the optimum the more the displacement is similar to the classical immiscible displacement, with droplets and interfaces being rather confined to the actual displacement front.

Coming closer to optimum conditions at 2 wt.% NaCl, lamella can easily be formed, but are indeed unstable, not for the above given reason of missing capillary forces at ultralow IFT conditions; the oil phase confined in the
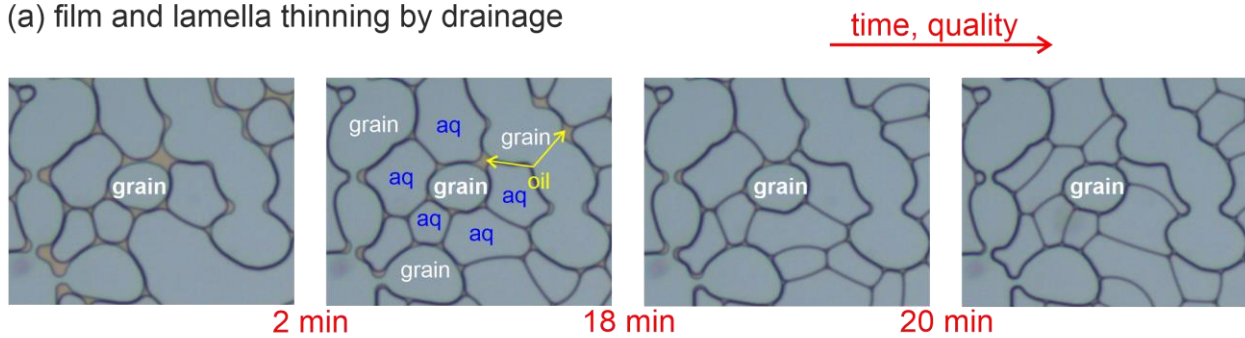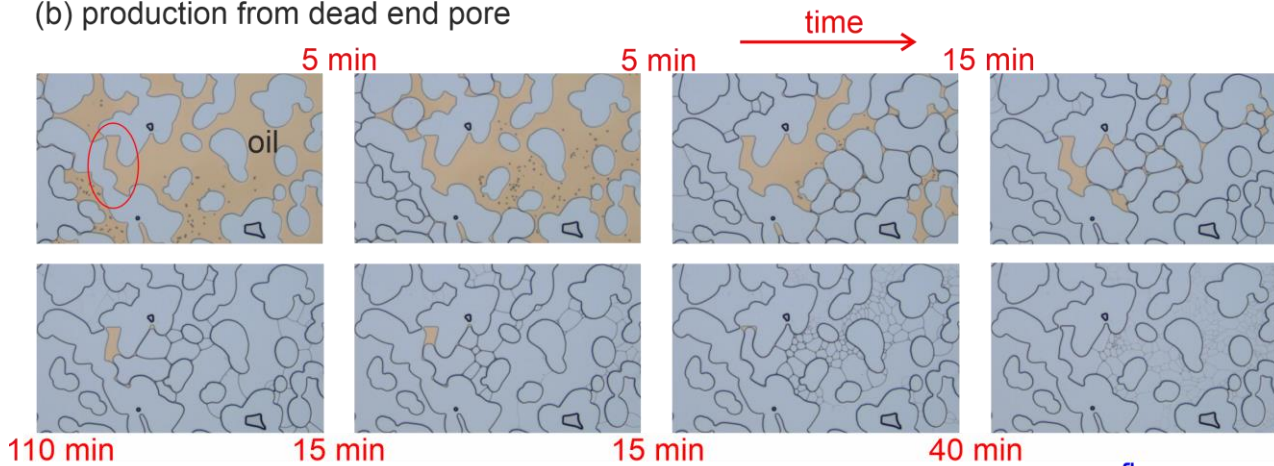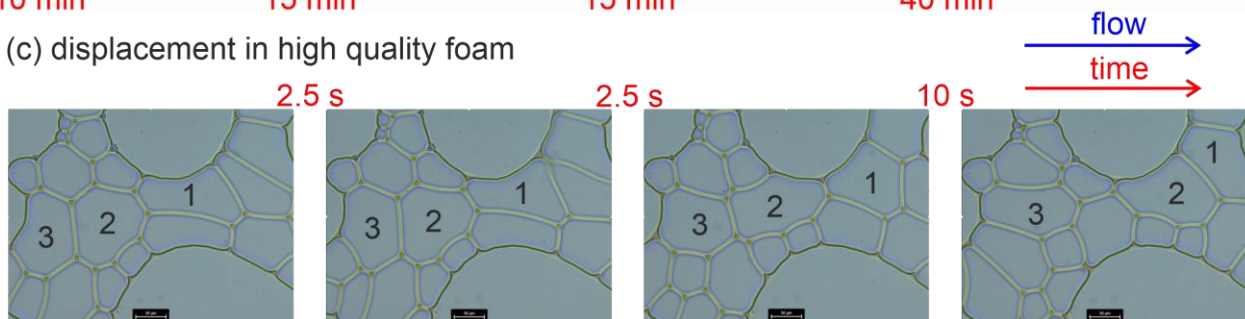
Figure 8 : Oil mobilization mechanisms. (a) Film thinning and drainage process, which leads to a reduction in foam quality. (b) Immiscible displacement and production from a dead-end pore. (c) Oil is transported as foam phase. The lamellae are oil-based and with the compartments, oil is transported as micro emulsion (compare to Figure 7).

lamella becomes progressively solubilized in the "aqueous" phase, which can be detected by the vanishing contrast in between compartments/bubbles and lamella, as seen in Figure 8 (b) and discussed in the following section.

5 Pore scale oil mobilization mechanisms

The foam-like structures consist of aqueous-phase and emulsion compartments of homogenous composition and the surrounding oil phase. Both phases are mobile and carry oil solubilized in water as seen from fluorescence microscopy and in the lamella. The images presented in the previous section show this foam-like phase is (a) displacing initially trapped oil and (b) is increasing its foam quality by displacement. The underlying mechanisms are visualized and explained in the following examples.

5.1 Film thinning and film drainage

The key mechanisms for oil displacement in the foam phase is the ability of the system to drain the oil films covering the initially oil-wet solid surfaces by forming lamella. This effect is illustrated in Figure 8 (a), referring to the 3 wt.%-NaCl case in the over-optimum. The image shows a time series from left to right, in which the "foam quality" is increasing, respectively the oil saturation is decreasing. Likely due to injection pressure, the compartments are coming close together, draining the oil phase in between them – the foam quality is increasing. The oil volumes may disappear into newly formed lamella, leading to an increasing compartmentalization and increasing interfacial area. The lamella, vortices, contacts to the solid and oil films became thinner over time forming a high-quality foam with a minimum oil phase forming the boundaries.

As predominantly observable in the videos (supp. mat.), moving lamella often means stretching of those, which requires additional material. This material is supplied from the oil films covering the solid surfaces via the "plateau borders", which apparently is thinning the oil films.

There is a third mechanism thinning or even removing the oil films. In the course of the displacement, oil films are continuously contacted with injection fluid, continuously solubilizing it. We may say that during the process – especially near optimum conditions – the foam quality is increasing, which coincides with the observation on the larger scale as discussed in the previous section. Ultimately, the oil film may disappear, which may be interpreted as wettability change, since the surfaces are ultimately covered by the aqueous phase. However, solubilization of lamella and films many not play a dominant role in the present case over optimum (Figure 8 (a)) and on the time scale of observation. Solubilization would lead to a vanishing optical contrast between lamella and films with respect to the compartments as discussed in the following.

5.2 Production from dead-end pores

The production from dead-end pores – or maybe in general the production from capillary trapped oil volumes – may be described by a series of mechanisms. This series is illustrated in Figure 8 (b): The dead-end pore described is marked by the red oval in the first image of the time series. The situation refers to the 2 wt.% case. In a first step, a compartment of the aqueous phase is penetrating into the pocket by the injection pressure, displacing the oil from the dead end. This displacement is possible even if the invading phase is "sealing" the dead-end. This is because in the oil wet system the oil is allowed to escape via the oil films covering the solid surfaces. These films are connected via the plateau borders to the lamella and therefore the initially trapped oil can be transported and transformed to new lamella forming a foam-like phase. The oil displacement happens finally in the form of the oil-based foam. This mechanism has been observed for all systems outside and near the optimum salinity. The major difference between sub-optimal and optimal conditions is that near optimum, the foam phase, respectively the lamellae are progressively solubilized on their way through the porous medium forming a single-phase fluid, which is nicely illustrated in the last to images of the time series and the respective videos at optimum conditions (supp. mat.). Outside optimum, the lamellae are generally more stable. This solubilization is most efficient near the optimum, leading to the highest ultimate recovery factor.

5.3 Oil displacement in high quality foam

The time evolution of the high-quality foam phase is shown in Figure 8 (c). Even if the pattern is qualitatively not changing, the individual compartments transport solubilized oil, and oil is transported by moving lamella. The images, again, shows a time series and three of the compartments are marked for tracking them. On the way through the image series, lamella, vertices and plateau borders continuously disappear and are created. This may best be seen in the respective video in the supplementary material (supp. mat.).

6 Summary and Conclusions

In the present paper we investigate the phase behavior and the development of emulsion phases during surfactant flooding. For this, we make use of the high spatial and temporal resolution of microfluidics and we use complementary contrast agents of optical and fluorescence microscopy in order to highlight the oil solubilized in the invaded phase and the remaining oil phase, separately.

The surfactant flooding experiments were carried out for different NaCl concentrations in order to tune the phase behavior across an optimum as examined in classical phase behavior experiments and by the remaining oil saturation from the displacement experiments.

During the flooding, emulsion phases with substantially different textures developed in time and space. A sequence of loose droplets/ganglia at the flood front developed into a foam-like phase. Comparing the texture to classical foam flooding experiments in literature, this sequence may be described as a foam phase with varying foam quality.

By combining optical with fluorescence microscopy, oil displacement mechanisms could be identified and described. A central role plays the drainage, respectively the thinning of oil-films and lamellae during displacement, which leads to the quality increase and to oil transportation. Flow in thin films have also been identified as mechanism to successively drain oil trapped in dead end pores. On top of the displacement of the pure oil phase, oil is transported solubilized in the injection water, which is compartmentalized in the foam structure. By using fluorescence microscopy, the solubilized oil content could be quantified.

The major qualitative difference between near-optimum and sub-optimum conditions is the degree to which oil is solubilized. Near optimum, lamellae and films progressively disappear on their way through the porous medium making a transition to a single phase. Further away from the optimum, the foam-like phase is rather confined to the region close to the flood front and for the highest investigated salinity in the over optimum, only some interfaces were observed.

Acknowledgements

Supporting Material

Videos as supporting material are provided under:
https://oc.unileoben.ac.at/index.php/s/N4bCc0NEhnW9D6h

References

[1] L. W. Lake, R. T. Johns, W. R. Rossen and G. A. Pope, Fundamentals of Enhanced Oil Recovery, SPE, 2014.

[2] M. Lawrence and G. D. Rees, "Microemulsion-based media as novel drug delivery systems," *Advanced Drug Delivery Reviews,* vol. 45, no. 1, pp. 89-121, 2006.

[3] D. J. McClements, "Crystals and crystallization in oil-in-water emulsions: Implications for emulsion-based delivery systems," *Advances in Colloid and Interface Science,* vol. 174, pp. 1-30, 2012.

[4] L. Sagalowicz and M. E. Lese, "Delivery systems for liquid food products," *Current Opinion in Colloid & Interface Science,* vol. 15, no. 1-2, pp. 61-72, 2010.

[5] A. Bera, "Microemulsions: a novel approach to enhanced oil recovery: a review," *https://link.springer.com/journal/13202,* 2015.

[6] I. B. Ivanov and P. A. Kralchevsky, "Stability of emulsions under equilibrium and dynamic conditions," *Colloids and Surfaces A: Physicochemical and Engineering Aspects,* vol. 128, no. 1-3, pp. 155-175, 1997.

[7] E. Unsal, S. Oedai and J. v. Wunnik, "Microemulsion Formation and its Effects on in Situ Rheology During ASP Corefloods: Scouting Study," *SPE,* 2016.

[8] M. Tagavifar, K. Xu, S. H. Jang, M. T. Balhoff and G. A. Pope, "Spontaneous and Flow-Driven Interfacial Phase Change: Dynamics of Microemulsion Formation at the Pore Scale," *Langmuir,* 2017.

[9] H. Ott, A. Kharrat, M. Borji and P. Arnold, "Fluid-phase topology of complex displacements in porous media," *Phys. Rev. Research,* 2020.

[10] E. Unsal, M. Broens and R. T. Armstrong, "Pore Scale Dynamics of Microemulsion Formation," *Langmuir,* 2016.

[11] M. Broens and E. Unsal, "Emulsification kinetics during quasi-miscible flow in dead-end pores," *Advances in Water Resources,* 2018.

[12] Y. Alzahid, P. Mostaghimi, M. Ebrahimi Warkiani, V. Joekar-Niasar, N. Karadimitriou and R. T. Armstrong , "Alkaline Surfactant Polymer Flooding: What Happens at the Pore Scale?," *SPE,* 2017.

[13] Y. A. Alzahid, P. Mostaghimi, S. D. Walsh and R. T. Armstrong, "Flow regimes during surfactant flooding: The influence of phase behaviour," *Fuel,* 2019.

[14] P. A. Winsor , "Hydrotropy, solubilisation and related emulsification processes," *Trans. Faraday Soc,* 1948.

[15] R. N. Healy, R. L. Reed and J. Clarence W. Carpenter, "A Laboratory Study of Microemulsion Flooding," *SPE,* 1975.

[16] G. Willhite, D. Green, D. Okoye and M. Looney, "A Study of Oil Displacement by Microemulsion Systems Mechanisms and Phase Behavior," *SPE,* 1980.

[17] D. Levitt, A. Jackson, C. Heinson, L. N. Britton, T. Malik, V. Dwarakanath and G. A. Pope, "Identification and Evaluation of High-Performance EOR Surfactants," *SPE Res Eval & Eng ,* 2009.

[18] N. Quennouz, M. Ryba, J.-F. Argillier, B. Herzhaft, Y. Peysson and N. Pannacci, "Microfluidic Study of Foams Flow for Enhanced Oil Recovery," *Oil &Gas Science and Technology,* 2014.

[19] C. Yeates, S. Youssef and E. Lorenceau, "New insights of foam flow dynamics in a high-complexity 2D micromodel," *Colloids and Surfaces A,* 2019.

[20] L. Labarre and D. Vigolo, "Microfluidics approach to investigate foam hysteretic behaviour," *Microfluidics and Nanofluidics,* 2019.